BULLETIN OF THE POLISH ACADEMY OF SCIENCES
TECHNICAL SCIENCES
Vol. 53, No. 4, 2005

Simulation of λ-phage DNA in microchannels using dissipative particle dynamics

V. SYMEONIDIS[1]*, G.E. KARNIADAKIS[1], and B. CASWELL[2]

[1]Division of Applied Mathematics, Brown University, Rhode Island, USA
[2]Division of Engineering, Brown University, Rhode Island, USA

Abstract. Dissipative Particle Dynamics (DPD) is a simulation method at mesoscopic scales that bridges the gap between molecular dynamics and continuum hydrodynamics. It can simulate efficiently complex liquids and dense suspensions using only a few thousands of virtual particles and at speed-up factors of more than one hundred thousands compared to Molecular Dynamics. Lowe's approach provides a powerful alternative to the usual DPD integrating schemes. Here, we demonstrate the details and potential of Lowe's scheme. We compute viscosity, diffusivity and Schmidt number values and we present comparison of wormlike chain models under shear with experimental and Brownian Dynamics results for λ-phage DNA.

Key words: dissipative particle dynamics (DPD), λ-phage DNA, microchannels.

1. Multiscale modelling

The Molecular Dynamics (MD) method is suitable for simulating very small volumes of liquid flow, with linear dimensions of the order of 100 nm or less and for time intervals of several tens of nanoseconds. It can deal effectively with nano-domains and is perhaps the only accurate approach in simulating flows involving very high shear where the continuum or the Newtonian hypothesis may not be valid. For length scales less than approximately ten molecules the continuum hypothesis breaks down for liquids [1], and MD should be employed to simulate the atomistic behaviour of such a system. For larger systems, however, multiscale approaches that rely on the efficiency of continuum-based discretizations have to be employed. To this end, the coupling of MD to Navier-Stokes equations can extend the range of applicability of both approaches and provide a unifying description of liquid flows from nano-scales to larger scales. Such effort has been underway by many research groups (e.g. Nie et al., 2004 [2], and references therein); however, the proposed algorithms are rather complicated and not fully satisfactory. An alternative, potentially very powerful and simple approach, is a method developed in the mid 1990s primarily in Europe: the dissipative particle dynamics (MD) method. It has features of both the MD and the lattice Boltzmann method (LBM) [3], and can be thought of as a coarse-grained version of MD, but it employs dissipative and stochastic forces to account for the eliminated degrees of freedom. The initial model was proposed by Hoogerbrugge & Koelman [4] as a simulation method to avoid the artifacts associated with traditional LBM simulations while capturing spatio-temporal hydrodynamic scales much larger than those achievable with MD.

The dissipative particle dynamics (DPD) model consists of particles which correspond to coarse-grained entities, thus representing molecular clusters rather than individual atoms. The particles interact with each other through a set of prescribed (conservative and stochastic) and velocity-dependent forces [4,5]. Specifically, there are three types of forces acting on each dissipative particle: (a) a purely repulsive conservative force, (b) a dissipative force that reduces velocity differences between the particles, and (c) a stochastic force directed along the line connecting the centers of the particles. The last two forces effectively implement a thermostat so that thermal equilibrium is achieved. Correspondingly, the amplitude of these forces is dictated by the fluctuation-dissipation theorem [5] that ensures that in thermodynamic equilibrium the system will have a canonical distribution. All three forces are modulated by a weight function which specifies the range of interaction or cut-off radius r_c between the particles and renders the interaction local.

A conceptual picture then of DPD is that of soft microspheres randomly moving around but following a preferred direction dictated by the conservative forces. DPD can be interpreted as a Lagrangian discretization of the equations of fluctuating hydrodynamics as the particles simultaneously follow the classical hydrodynamic flow while exhibiting thermal fluctuations. The consistency of the fluctuations is governed by the principles of statistical mechanics.

2. Complex fluids

Several complex fluid systems in industrial and biological applications (DNA chains, polymer gels, lubrication) are characterized by inherent time and length scales that range from the atomistic level to a millimeter and beyond, often spanning several orders of magnitude. Traditional molecular dynamics techniques attack the problem at the microscopic level, while continuum models may fail to capture smaller interactions because they resort to averaging techniques or pre-defined as-

*e-mail: sjoh0341@dam.brown.edu

sociation rules. Dilute polymer solutions are a typical example, since individual polymer chains form a group of molecules large by atomic standards but still governed by forces similar to intermolecular ones. Therefore, they form large repeated units exhibiting slow dynamics with possibly non-linear interactions (Fig. 1).

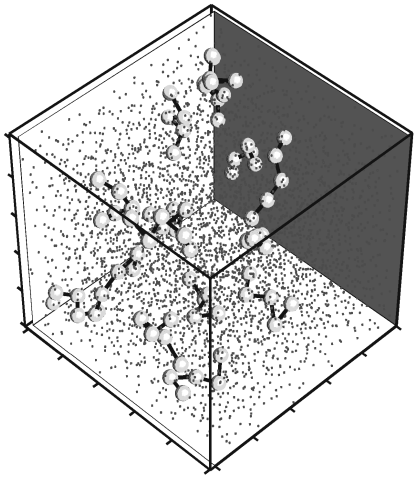

Fig. 1. Polymer chains (tethered spheres) suspended in a solvent of DPD particles (smaller dots)

The DPD method is very attractive for the computer simulation of polymer solutions, since by employing bead-spring representations of the polymer chains we can formulate and compare a variety of realistic conservative inter-bead forces. We focus on using the basic DPD framework in order to formulate, implement and compare different models for polymer chains in dilute solutions. In order to appreciate the potential and computational complexity of DPD, in the following section we summarize the governing equations for simple and complex fluids, and subsequently we present Lowe's scheme and physical results.

3. The DPD equations

The system consists of N particles having equal mass (for simplicity) m, positions $\mathbf{r}_i$, and velocities $\mathbf{u}_i$. The aforementioned three types of forces exerted on a particle i by particle j are given by

$$\mathbf{F}_{ij}^c = F^{(c)}(r_{ij})\mathbf{e}_{ij},$$
$$\mathbf{F}_{ij}^d = -\gamma\omega^d(r_{ij})(\mathbf{u}_{ij}\cdot\mathbf{e}_{ij})\mathbf{e}_{ij},$$
$$\mathbf{F}_{ij}^r = \sigma\omega^r(r_{ij})\xi_{ij}\mathbf{e}_{ij},$$

where $\mathbf{r}_{ij} = \mathbf{r}_i - \mathbf{r}_j$, $\mathbf{u}_{ij} = \mathbf{u}_i - \mathbf{u}_j$, $r_{ij} = |\mathbf{r}_{ij}|$ and the unit vector $\mathbf{e}_{ij} = \frac{\mathbf{r}_{ij}}{r_{ij}}$. The parameters γ and σ determine the strength of the dissipative and random forces, respectively, the ξ_{ij} are symmetric Gaussian random variables with zero mean and unit variance, and ω^d and ω^r are weight functions.

All forces act within a sphere of radius r_c, which defines the length scale of the system. By averaging the Lennard-Jones potentials or the corresponding molecular field over the rapidly fluctuating motions of atoms over short time intervals, an effective average potential [6] is obtained of the form shown in Fig. 2 that is a soft, repulsive-only interaction. A linear approximation of this is as follows [7]: $\mathbf{F}_{ij}^c = a_{ij}(1-r_{ij})\mathbf{e}_{ij}$ for $r_{ij} \le r_c = 1$ and is otherwise zero. Unlike the hard Lennard-Jones potential which is unbounded at $r = 0$, the soft potential employed in DPD has a finite value a_{ij} at $r = 0$. To find the value of a_{ij} we follow the process laid out by Groot & Warren [7] and Groot & Rabone [8], i.e., we match the dimensionless compressibility of the DPD system with that of the MD system, namely

$$\begin{aligned}\kappa^{-1}|_{\text{DPD}} &= \frac{1}{k_B T_{\text{DPD}}}\left[\frac{\partial p_{\text{DPD}}}{\partial \rho_{\text{DPD}}}\right]_{\text{T}} \\ &= \frac{1}{k_B T_{\text{MD}}}\left[\frac{\partial \rho_{\text{MD}}}{\partial \rho_{\text{DPD}}}\right]\left[\frac{\partial p_{\text{MD}}}{\partial \rho_{\text{MD}}}\right]_{\text{T}} = N_m\kappa^{-1}|_{\text{MD}}\end{aligned} \tag{1}$$

where ρ is the number density, $N_m = \frac{(\partial\rho)_{\text{MD}}}{(\partial\rho)_{\text{DPD}}}$ is the coarse-graining parameter , k_B is the Boltzmann constant and T the temperature of the system. We note that "DPD" refers to simulation and that in MD we have $N_m = 1$. Then, from an empirical equation of state for DPD fluids, Groot & Warren [7] obtain $a_{ij} \equiv a$ through

$$\kappa^{-1}|_{\text{DPD}} \approx 1 + 0.2\frac{a\rho_{\text{DPD}}}{k_B T_{\text{DPD}}}.$$

By matching the diffusion constant (D_{DPD}) in the DPD simulation with that of water (D_{water}) we find the DPD time scale as

$$\tau = \frac{N_m D_{\text{DPD}} r_c^2}{D_{\text{water}}} \propto N_m^{5/3}.$$

This time scale and the soft potential explain why the DPD method is several orders of magnitude faster than straightforward MD. With respect to the latter, the soft potential removes the "caging effect" of an atom so that the diffusivity of atoms is increased by a factor of 1000, depending on the thermostat. We note that Lowe's [9] approach, which employs an Andersen thermostat, does not decrease the Peclet number. The effect of the time scale is to decrease the corresponding CPU time in proportion to the coarse-graining parameter N_m; hence the total speed-up with respect to MD is $1000 \times N_m \times N_m^{5/3}$ for a given system volume. Thus, for $N_m = 5$ and 10 the speed-up factor is 73,000 and 464,000, respectively!

The time evolution of DPD particles is described by Newton's law

$$d\mathbf{r}_i = \mathbf{u}_i\delta t; \qquad d\mathbf{u}_i = \frac{\mathbf{F}_i^c\delta t + \mathbf{F}_i^d\delta t + \mathbf{F}_i^r\sqrt{\delta t}}{m_i},$$

where $\mathbf{F}_i^c = \sum_{i\neq j}\mathbf{F}_{ij}^c$ is the total conservative force acting on particle i; $\mathbf{F}_i^d$ and $\mathbf{F}_i^r$ are defined similarly. The random force, which represents Brownian motion, appears with a factor of $\sqrt{\delta t}$ in the velocity increment. The dissipative and random forces, characterized by strengths $\omega^d(r_{ij})$ and $\omega^r(r_{ij})$ respectively, are coupled through the fluctuation-dissipation theorem [5] as follows:

$$\omega^d(r_{ij}) = \left[\omega^r(r_{ij})\right]^2 = \max\{(1-\frac{r_{ij}}{r_c})^2, 0\}$$
$$\sigma^2 = 2\gamma k_B T.$$

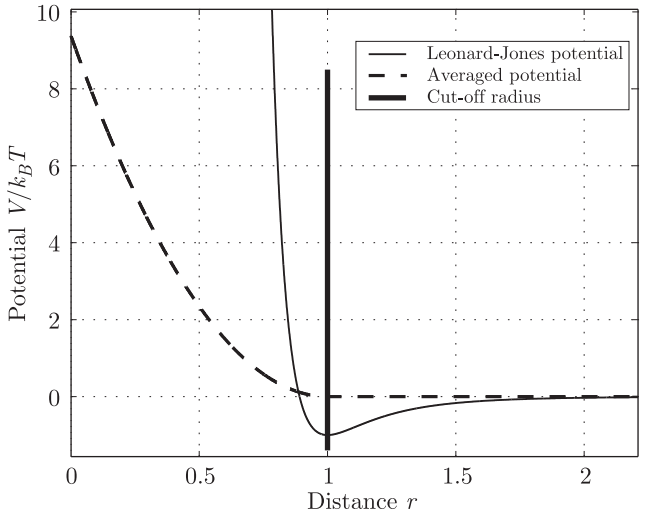

Fig. 2. Lennard-Jones potential and the soft-repulsive potential which results after averaging

4. Lowe's scheme

The most widely used DPD integrating scheme is the velocity-Verlet algorithm [10] – a popular version of which is outlined by Groot and Warren [7]. Lowe's algorithm, on the other hand, introduced in 1999 [9,11] is a scheme based on the Andersen thermostat [12] with the particle velocities corrected every timestep using the Maxwell velocity distribution. In absence of conservative forces, which are integrated in the velocity-Verlet manner, the scheme is shown to be independent of the chosen timestep Δt [11]. The core operation in Lowe's method involves re-equilibration of the particle momenta at one step with an updated inter-particle relative velocity drawn from a Gaussian distribution.

The method conserves momentum and introduces an extra parameter Γ so that in the limiting case of $\Gamma \times \Delta t \approx 1$ thermalization/dissipation occurs every time-step. Peters [13] recently introduced a modification of Lowe's scheme by keeping the centroid velocity of a particle-pair unchanged before and after the re-equilibration. This results in an attractive scheme, still independent of the chosen time-step (as opposed to the Verlet approach) that also discretizes the original DPD equations. Here we outline the basic Lowe scheme in Table 1. The fundamental difference between Lowe's and the velocity-Verlet scheme is that dissipative and random forces are not explictly calculated in the former.

Table 1
Overview of the traditional Lowe's approach for a polymer system

Γ: thermalization parameter

- ► $\mathbf{r}_{s_i} \longleftarrow \mathbf{r}_{s_i} + (\Delta t)\mathbf{u}_{s_i} + \frac{(\Delta t)^2}{2m}\mathbf{F}^c_i$: SOLVENT
- ► $\mathbf{r}_{p_i} \longleftarrow \mathbf{r}_{p_i} + (\Delta t)\mathbf{u}_{p_i} + \frac{(\Delta t)^2}{2m}\left[\mathbf{F}^c_i + \mathbf{F}^p_i\right]$: POLYMER
- ► $\forall_{(i,j)} \quad \widehat{\mathbf{F}}^c_i \begin{pmatrix} \mathbf{r}_s \\ \mathbf{r}_p \end{pmatrix}$: SOLVENT, POLYMER
- ► $\forall_{(i,j)} \quad \widehat{\mathbf{F}}^p_i(\mathbf{r}_p)$: POLYMER
- ► $\mathbf{u}_{s_i} \longleftarrow \mathbf{u}_{s_i} + \frac{\Delta t}{2m}\left[\mathbf{F}^c_i + \widehat{\mathbf{F}}^c_i\right]$: SOLVENT
- ► $\mathbf{u}_{p_i} \longleftarrow \mathbf{u}_{p_i} + \frac{\Delta t}{2m}\left[\left(\mathbf{F}^c_i + \mathbf{F}^p_i\right) + \left(\widehat{\mathbf{F}}^c_i + \widehat{\mathbf{F}}^p_i\right)\right]$: POLYMER

- ► $\forall\, N_p$ distinct pairs i, j such that $r_{ij} < r_c$: SOLVENT, POLYMER
  - Generate a Gaussian ξ_{ij} with $\mu = 0, \sigma^2 = 1$
  - Form $\mathbf{u}^\circ_{ij} \cdot \mathbf{e}_{ij} = \xi_{ij}\sqrt{\frac{2k_BT}{m}}$
  - Generate a uniform distribution ψ_{N_p}
  - If $\psi_{N_p} < \Gamma \times \Delta t \leq 1$:

$$\begin{aligned} &2\boldsymbol{\Delta}_{ij} = \mathbf{e}_{ij}(\mathbf{u}^\circ_{ij} - \mathbf{u}_{ij}) \cdot \mathbf{e}_{ij} \\ &\mathbf{u}_i \longleftarrow \mathbf{u}_i + \boldsymbol{\Delta}_{ij} \\ &\mathbf{u}_j \longleftarrow \mathbf{u}_j - \boldsymbol{\Delta}_{ij} \end{aligned}$$

- ▷ $\mathbf{F}^c_i \longleftarrow \widehat{\mathbf{F}}^c_i$: SOLVENT, POLYMER
- ▷ $\mathbf{F}^p_i \longleftarrow \widehat{\mathbf{F}}^p_i$: POLYMER

- ▷ Analyzer

5. The wormlike chain

Unlike the MD equations, the DPD equations are stochastic and nonlinear since the dissipative force depends on the velocity. The conservative forces present in the usual DPD equations can be tailored in such a way so as to describe a variety of interactions – e.g. Lennard-Jones (LJ), Hookean dumbbells, Finitely Extensible Non-Linear Elastic (FENE) springs and van der Waals forces – as long as they are derivable from a given potential $V(r_{ij})$.

Figure 1 shows polymeric chains moving freely in a DPD solvent of N particles. These chains consist of beads (DPD particles) subject to the standard DPD forces: soft repulsive (conservative), dissipative and random. In addition to these forces, they are subject to intra-polymer forces, arising from different combinations of spring laws between consecutive beads on a chain (bonded interactions) and possibly excluded volume repulsions (non-bonded interactions).

Polymer models of biological importance (DNA, proteins) have been known to be governed by stiff interactions. The worm-like chain [14–16] can be thought of as a continuous curve in three-dimensional space. Of importance is the persistence length λ_p, which is a measure of the chain's stiffness and is the average length over which the orientation of a curve segment does not change ("persists"). We will focus on the bead-spring representation of the model, which approximates a portion of the worm-like chain with a force law given by the Marko-Siggia [17] expression

$$F^{(c)} = \frac{k_B T}{\lambda_p}\Big[\frac{1}{4(1-R)^2} - \frac{1}{4} + R\Big],$$

where

$$R = \frac{|\vec{r}_i - \vec{r}_{i-1}|}{L_{\rm spring}} = \frac{r}{L_{\rm spring}} \quad i = 2, 3, 4, ..., M$$

and $L_{\rm spring}$ is the maximum allowed length for each chain (spring) segment. The expression is accurate for large values of the ratio $L_{\rm spring}/\lambda_p$ and exact as $r \to 0$ or $r \to L_{\rm spring}$.

The Marko-Siggia spring law is an averaged quantity, locally approximating flexible rods. The derivation of the formula accounts for coarse-graining microscopic elements of a long chain (such as bead-rod), by use of statistical mechanics. However, in order to use the Marko-Siggia law in molecules with more than two beads (dumbbells), some authors [18] account for the different stiffness of the beaded counterparts by altering the persistence length λ_p of the sub-chains. Detailed analysis of such arguments [19] has shown that it is possible to minimize the errors arising by the introduction of beads and sub-chains. Throughout this work we will adopt the analysis presented in [19] for stained λ-phage DNA molecules assumed to have $L = 21.1$ μm (fully extended length) and $\lambda_p = 0.053$ μm (persistence length). The correction we will apply will linearly approximate the ratio of effective to true persistence length, for three different regions of the extension: low force, half-extended spring and high-force regimes. More specifically, we define the ratio

$$\lambda^\star = \frac{\lambda_p\,[\text{EFFECTIVE}]}{\lambda_p\,[\text{TRUE}]}$$

so that when $\lambda^\star = 1$ no correction is applied. The tables in [19] suggest a high, medium and zero correction for the low-force, half-extension and high-force regions respectively. We go one step further to introduce a linear fit to the suggested correction values for N-bead chains:

$$\lambda^\star \approx (1.0 - \hat{z}) \times 0.022 \times (N-1) + 1, \quad \text{if} \quad N \le 20$$

$$\lambda^\star \approx (1.0 - \hat{z}) \times 0.025 \times (N-1) + 1, \quad \text{if} \quad N > 20,$$

where $0 \le \hat{z} \le 1$ is the instantaneous fractional extension of the whole molecule in the stretching direction. The above expressions approximate fairly accurately the values given in [19] and are implemented in all instances of $N > 2$ for the Marko-Siggia spring force in this work.

6. Shear response of wormlike chains

The results presented in this section aim to simulate the response of λ-phage DNA molecules under steady shear, and compare the DPD results with corresponding results from Brownian Dynamics (BD) and experimental data. The wormlike chain (WLC) described in section 5 is used for all DNA simulations and Underhill & Doyle's [19] persistence length (λ_p) correction always applies to our results for $M > 2$. Bouchiat's [20] correction for the dumbbell case produced statistically similar results to the original Marko-Siggia (M-S) model. Since the λ_p correction studies in [19] were done with the M–S formula, we do not use Bouchiat's version.

DNA molecules under steady shear have been extensively studied in experimental [21] and computational [22,23] works. In 1999, Smith et al. [21] performed a benchmark study of λ-DNA molecules in uniform shear flow of shear rates $\dot{\gamma} < 4.0\frac{1}{s}$ employing a $\sim$ 50 μm gap in solvents with viscosities $\mu = 60, 220\ cP$. These stained bacteriophage molecules have a contour length $L \sim 21$ μm and longest relaxation times of 6.3 s (in the 60 cP solution) and 19 s (in the 220 cP solution). A typical molecule contains roughly 400 persistence lengths and hence can be considered flexible. Using DPD we investigated the dynamics of a single WLC. The moving boundaries at $y = 0, y = L_y$ are modeled using Lees-Edwards boundary conditions [24]: particles leaving the domain at $y = 0, L_y$ are advanced/retarded by an increment of $\Delta r = U_x t, -U_x t$ respectively in the $x-$direction, where t is the time elapsed from an appropriate origin of times and U_x denotes twice the shear velocity of each boundary. Moreover, the velocity of the particle is increased/decreased by $U_x, -U_x$, accounting for both the imposed boundary condition and the velocity discontinuity between the two walls. This correction is essential, since the dissipative forces depend on the relative pairwise velocities. The rest of the boundaries are treated periodically for all the solvent DPD particles. To avoid unphysical periodicity artifacts, polymer beads only undergo an elastic collision in the y-direction: $(u, v, w)_{\rm BEAD} \to (u, -v, w)_{\rm BEAD}$ and $r_y \to r_y - (\Delta t) v_{\rm BEAD}$. Different chain sizes were accommodated by storing the polymer coordinates without mapping them back in the original domain. This allowed the intra-polymer forces to be calculated properly, while the collective

solvent-solvent and polymer-solvent interactions were calculated with the mapped (periodic) images. The effect of the simulation box size $L_x \times L_y \times L_z$ for the presented results was investigated and proved to be negligible. For the results shown, a periodic box of dimensions $10 \times 20 \times 5$ was used in a fluid of 4000 DPD particles. The conservative force amplitude was fixed to $a_{ij} = 75\ k_B T/\rho$, as in [7].

In order to properly simulate λ-phage DNA molecules under steady shear, we define the dimensionless Weissenberg number of the flow as $We = \dot{\gamma}\tau$, for a shear rate $\dot{\gamma}$. Here, τ is the polymer's longest relaxation time, which is computed by fitting an exponential analytical curve to the average mean-square extension; this is not necessarily the end-to-end value. This approach provides a relaxation time nearly the same (within 10%) with that obtained by fitting the late-time tail of the mean-square radius of gyration $\langle {R_g}^2 \rangle$. Figure 3 shows the fitted results. The calculated mean-square extension of an initially 30%-extended chain was fitted with $\langle x^2 \rangle = \langle x^2 \rangle_0 + {x_i}^2 e^{-t/\tau}$ to obtain the chain relaxation time τ. Here, ${x_i}^2$ is the initial stretch and $\langle x^2 \rangle_0$ is the equilibrium value. Equating the area under both curves fixed the free parameter of the fit. Figure 4 shows the calculated average molecular (maximum projected) extension and the experimental data [21] versus We, with varying bead numbers and corresponding relaxation times. The asymptotic value for 20 beads (≈ 0.51) is in agreement with the corresponding one (0.47) from BD calculations [22]. Remarkably, the results for the average extension are not so sensitive to coarse-graining, i.e. the number of beads used for constant L, in the tested range. The self-consistency of the parameters was verified from the equilibrium mean-square end-to-end distance of a 2-bead dumbbell, computed as $\langle S^2 \rangle \approx 8.56$, in close agreement with the theoretical value of 8.92 given by [16] $\langle S^2 \rangle = 2L_{\rm sp}\lambda_p \left(1 - \frac{\lambda_p}{L_{\rm sp}}(1 - e^{-L_{\rm sp}/\lambda_p})\right)$. While most curves presented in Fig. 4 employ the widely used velocity-Verlet scheme for time integration, we have also included results for 2 beads using Lowe's method with $\Gamma = 4.5$. We will revisit the topic but we digress in the next section to discuss diffusion and the effect of Schmidt number (Sc) in the DPD simulations.

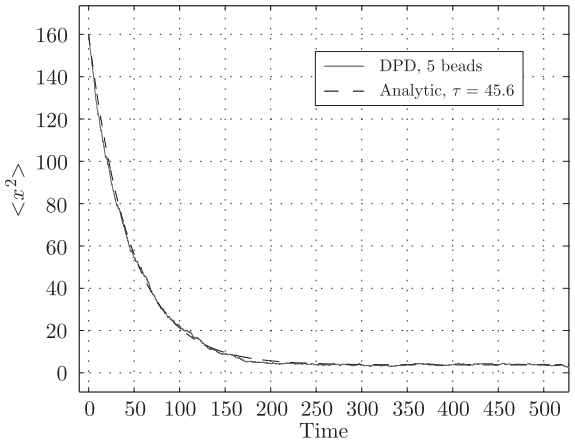

Fig. 3. Decay of the average mean-square extension $\langle x^2 \rangle$ and the corresponding exponential fit for a wormlike chain of 5 beads in a Newtonian solvent using Lowe's method ($\Gamma = 4.5$)

7. Dynamics: diffusion and viscosity

The characterization of the simulated fluid in DPD is of major importance for the understanding of the strengths and weaknesses of the method. In this section we examine fundamental quantities, such as kinematic viscosity $\nu = \mu/\rho$ and diffusion coefficient D_T and their dependence on the specific parameters of each DPD integrating scheme.

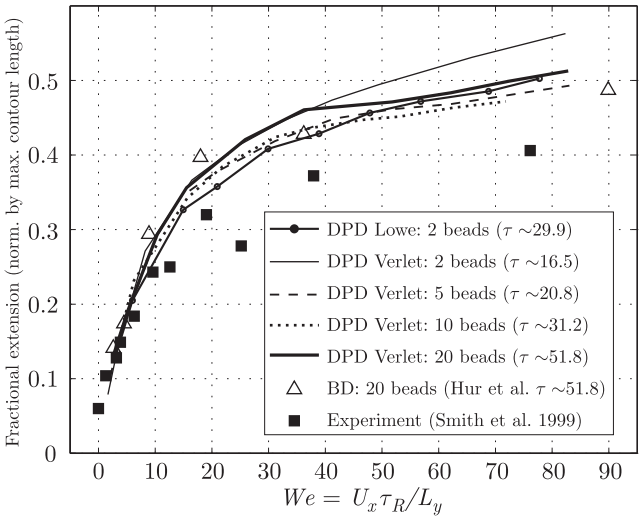

Fig. 4. Mean WLC fractional extension versus We compared to BD [22] and DNA experiments [21] data. The results presented use Groot & Warren's [7] velocity-Verlet ($\sigma = 3$) and Lowe schemes ($\Gamma = 4.5$)

The peculiar velocity $\widetilde{\mathbf{u}}_i$ of particle i is defined as $\widetilde{\mathbf{u}}_i = \mathbf{u}_i - \bar{\mathbf{u}}(\mathbf{x})$, where $\bar{\mathbf{u}}(\mathbf{x})$ is the stream velocity at position $\mathbf{x}$. For a system of N particles of mass m_i each, we define the $\alpha\beta$-component of the stress tensor through the Irving-Kirkwood formula [25]

$$S_{\alpha\beta} = -\frac{1}{L_x L_y L_z}\left\langle \sum_{i=1}^{N} m_i \widetilde{u}_{i\alpha}\widetilde{u}_{i\beta} + \sum_{i=1}^{N}\sum_{j>i}^{N} r_{ij\alpha} F_{ij\beta} \right\rangle, \tag{2}$$

where $F_{ij\beta}$ is the β-component of the net force acting on particle i due to particle j, and $r_{ij\alpha}$ is the α-component of their relative position vector. It is interesting to note here that equation [2] is directly applicable in its current form to the velocity-Verlet method but not Lowe's scheme, which lacks explicit calculation of dissipative/random forces. To this end, we propose a modification of Eq. 2 to incorporate the velocity re-equilibrations $\mathbf{\Delta}_{ij}$ in Lowe's scheme interpreted as an additional force term:

$$S_{\alpha\beta} = -\frac{1}{L_x L_y L_z}\left\langle \sum_{i=1}^{N} m_i \widetilde{u}_{i\alpha}\widetilde{u}_{i\beta} + \sum_{i=1}^{N}\sum_{j>i}^{N} r_{ij\alpha} F_{ij\beta} + \sum_{i=1}^{N}\sum_{j>i}^{N} m_i r_{ij\alpha}\frac{\Delta_{ij\beta}}{\Delta t} \right\rangle, \tag{3}$$

where Δt is the simulation timestep. The dynamic viscosity μ of the fluid is determined under shear through the total shear

stress S_{xy} (x is the direction of the shear and y the wall-normal direction) through

$$\mu = \frac{S_{xy}}{\dot{\gamma}}, \qquad \dot{\gamma} = \frac{U_x}{L_y},$$

and therefore the kinematic viscosity is $\nu = \frac{\mu}{\rho} = \frac{\mu L_x L_y L_z}{N}$. Here, $\dot{\gamma}$ is not to be confused with the dissipative force coefficient γ.

In this work we will, however, use a different approach for calculating the viscosity. Backer et al. [26] suggested the periodic Poiseuille flow method, which consists of simply superimposing a constant force $g_x, -g_x$ in the x-direction for all particles i with $\mathbf{r}_{i_y} > L_y/2$, $\mathbf{r}_{i_y} < L_y/2$ respectively. Then, for a periodic simulation box of length L_y in the $y-$direction, number density ρ, velocity profile $U(y)$ in the x-direction and dynamic viscosity μ the following formula holds:

$$\frac{\rho g_x (\frac{L_y}{2})^2}{12\mu} = \frac{2}{L_y} \int_{y=0}^{y=\frac{L_y}{2}} U(y) dy.$$

Regarding the Poiseuille profile method, it is interesting to note that:

1. It eliminates possible artificial side-effects from imposition of other types of boundary conditions, since it results in a fully periodic flow with all the advantages spatial periodicity has to offer combined with a Poiseuille profile.

2. Both opposite Poiseuille profiles can be used to obtain better ensemble averages.

3. Backer et al. [26] have demonstrated that it is more accurate than other already existing methods.

4. Our studies for both velocity-Verlet and Lowe's methods indicate a negligible disagreement of $\mathcal{O}(10^{-4})$ between the computed viscosity values via the shear stress and Poiseuille flow methods, rendering both methods equivalent for all practical purposes.

Figure 5 shows such a profile with the corresponding averaged one, together with the parabolic least-squares fit. The area under the right curve can be calculated either by directly integrating the fitted quadratic or by standard integration rules. All results presented here use analytic integration of the fitted quadratic.

The velocity autocorrelation function (VAF) can reveal information for the underlying nature of a dynamical process. We construct it as follows: Given an appropriate origin of time, we denote the value of all three components of the velocity vector as $\mathbf{u}|_{t=0} = \{u|_{t=0}, v|_{t=0}, w|_{t=0}\}$. The velocity components at an arbitrary instant $0 \leq t = T$ are recorded, and the scalar quantity

$$C_u|_{t=T} = \frac{1}{N} \sum_{i=1}^{N} \mathbf{u}|_{t=0} \cdot \mathbf{u}|_{t=T}$$

is the VAF; for short, we write $C_u(t) = \langle \mathbf{u}_i(0) \cdot \mathbf{u}_i(t) \rangle$. The VAF provides valuable information about the system's underlying frequencies, and when it decays to zero as $t \to \infty$, it can be integrated to calculate the diffusion coefficient D_T:

$$D_T = \frac{1}{3} \int_{t=0}^{t=\infty} C_u(t) \quad dt.$$

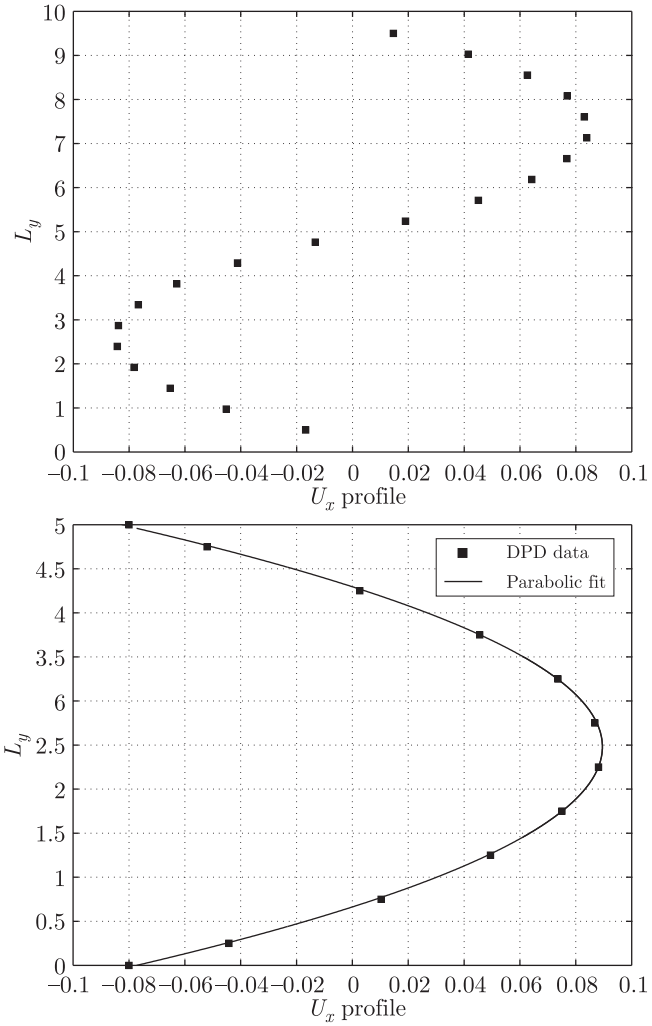

Fig. 5. Sample dual parabolic (up) and reflected and fitted (down) profiles

This type of definition of a transport coefficient (such as D_T) through an integral of a correlation function is a Green-Kubo relation [1]. D_T may also be calculated through the mean-square displacement of each DPD particle. In practice, the initial value $\mathbf{u}|_{t=0}$ is reset during a simulation numerous times in order to collect meaningful ensemble averages that can be easily integrated. If the timestep is relatively small ($\delta t \approx 0.01$) the integral can be accurately calculated using a standard trapezoidal or midpoint rule.

The fundamental differences between the velocity-Verlet and Lowe's scheme manifest themselves in the values of the diffusion coefficient D_T, the viscosity ν and eventually the Schmidt number $Sc = \frac{\nu}{D_T}$ characterizing the simulated fluid. Groot & Warren [7] had shown that the velocity-Verlet method for a number density $\rho = 3$ and a dissipation amplitude $\gamma = 6.75$ produced Schmidt number values close to those predicted by the theory, but extremely small compared to real fluids (three orders of magnitude smaller). Our calculations (not shown here) reveal that for $\sigma \in [1, 5.5]$ the Schmidt number for the velocity-Verlet method does not exceed the value of 3, see [27]. It is worth mentioning that the Schmidt number for the velocity-Verlet method is estimated [28,7] to follow

$Sc \sim \frac{1}{2} + (2\pi\gamma\rho r_c^4)^2/70875 k_B T$. This expression makes it clear that the corresponding achievable values are not in the same order of magnitude as Lowe's scheme for comparable CPU requirements.

7.1. The Schmidt number for Lowe's scheme ($\delta t = 0.001, 0.01$). In order to investigate the effect of Lowe's thermalization parameter Γ on the fluid, we compute D_T, ν and Sc for a wide range of values. Figure 6 shows the computed diffusion coefficient, viscosity and Schmidt numbers for a 4000-particle fluid, in a $10 \times 10 \times 10$ sized box with a time-step $\delta t = 0.01$ and a conservative force coefficient $a_{ij} = 75 k_B T/\rho$. For the viscosity calculations we apply a constant force of magnitude $g_x = 1$, as previously described, to obtain a periodic Poiseuille profile. Groot & Warren [7] correctly argue that the velocity-Verlet scheme produces unrealistic values for Sc. The calculated value of $Sc = 1.00 \pm 0.03$ for $\sigma = 3.67, \rho = 3$ provided in [7] is in reasonable agreement with the one we compute ($Sc \sim 1.3$ for $\sigma = 3.5, \rho = 4$) [27].

We investigate the described system for Lowe's scheme, and its dependence on the parameter Γ. To this end, we perform one series of simulations with $\delta t = 0.001$ and one with $\delta t = 0.01$. However, Γ is varied so that $\Gamma \times \delta t \in [1, 1000] \times 0.001 = [0.001, 1]$ and $\Gamma \times \delta t \in [1, 100] \times 0.01 = [0.01, 1]$, respectively.

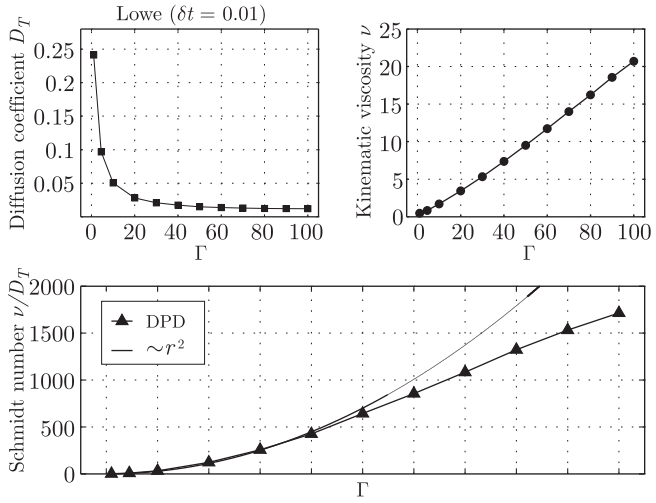

Fig. 6. Diffusion coefficient D_T (upper left), kinematic viscosity ν (upper right), and Schmidt number Sc (lower) plotted against Γ for Lowe's scheme with $\delta t = 0.01$. The Schmidt number is $\mathcal{O}(10^3)$. Here $k_B T = 1$

For an ideal dissipative gas, Lowe's thermostat is governed by two distinct timescales, as shown in [9]; a typical time t_1 it takes a particle to travel a distance r_c with a given velocity, and a typical time t_2 it takes the velocity correlations to decay. Assuming the latter to be dependent only on Γ, we have

$$t_1 = \sqrt{\frac{m r_c^2}{k_B T}}, \quad t_2 = \frac{1}{\Gamma} \quad \Rightarrow \quad \Lambda = \frac{t_2}{t_1} = \sqrt{\frac{k_B T}{m r_c^2 \Gamma^2}}.$$

Hence, under the assumption that the velocity correlations decay in time is $\tau_D \sim 1/\Gamma$, Lowe's scaling for the kinematic viscosity $\nu = \pi\rho\Gamma r_c^5/75m$ can be used to show that the Schmidt number

$$Sc = \frac{\text{VISCOSITY}}{\text{DIFFUSIVITY}} = \frac{\nu}{D_T} = \frac{\pi\rho\Gamma r_c^5/75m}{k_B T \tau_D/m} \sim \frac{1}{\Lambda^2} \sim \frac{\Gamma^2}{k_B T}.$$

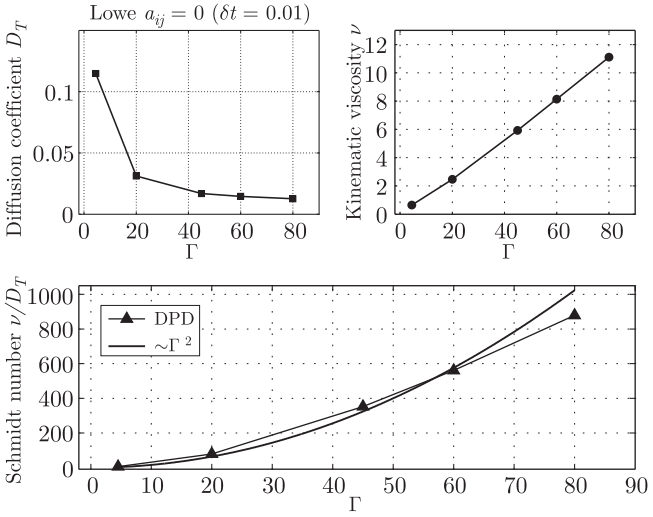

Fig. 7. Diffusion coefficient D_T (upper left), kinematic viscosity ν (upper right), and Schmidt number Sc (lower) plotted against Γ for Lowe's scheme with $a_{ij} = 0$ and $\delta t = 0.01$. The Schmidt number is $\mathcal{O}(10^3)$. Here $k_B T = 1$

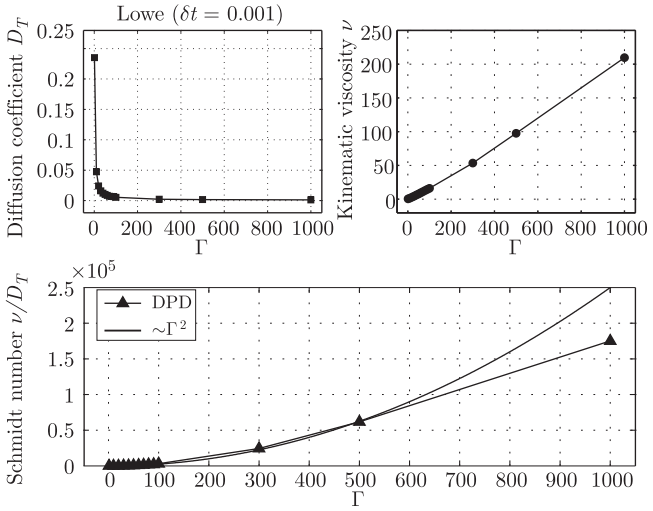

Fig. 8. Diffusion coefficient D_T (upper left), kinematic viscosity ν (upper right), and Schmidt number Sc (lower) plotted against Γ for Lowe's scheme with $\delta t = 0.001$. The Schmidt number is $\mathcal{O}(10^5)$. Here $k_B T = 1$

Lowe, in his original paper [9] derives the above scaling, and our results in both figures 6,8 verify this trend to be true for Γ values satisfying $0 \leq \Gamma \times \delta t \leq 0.5$. We anticipate the disagreement for large Γ values to improve if indeed an ideal gas ($a_{ij} = 0$) is simulated; in our simulations $a_{ij} = 75 k_B T/\rho$. Indeed, an ideal gas calculation of the above quantities was carried out and the quadratic dependence of the Schmidt number on Γ when $a_{ij} = 0$ is more pronounced – the results are shown

in Fig. 7. Lowe's method shows great potential in addressing the issue of realistic Sc values, since for the examined range of parameters the maximum Sc reaches values of $\mathcal{O}(10^5)$, i.e. five orders of magnitude larger than those of velocity-Verlet. Figures 6 and 8 show the dependence of the computed D_T, ν and Sc on Γ.

Here we note that the diffusion coefficient scales as $1/\Gamma$ and it is approximately independent of the size of the timestep despite the fact that the product $\Gamma \times \Delta t$ controls the thermalization process in Lowe's method. Figure 9 shows that the relaxation time for a 5-bead WLC scales roughly as $\sim \Gamma$ for Lowe's method. Intuition supports this, since viscosity scales linearly with Γ as well.

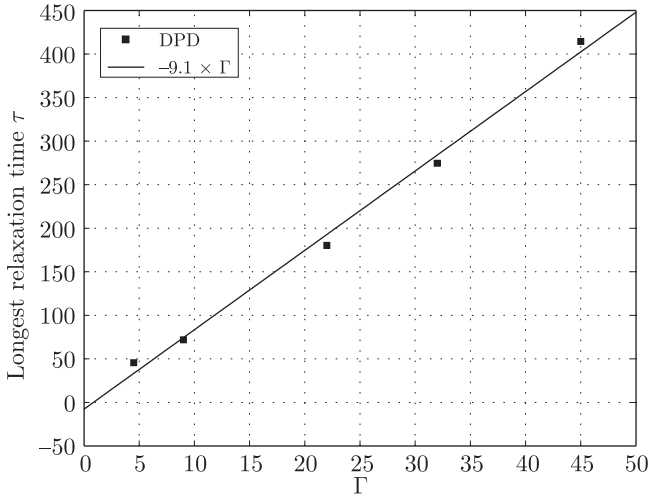

Fig. 9. Longest relaxation time τ for the wormlike chain (5 beads) plotted against Γ for $k_BT = 0.2$

8. Wormlike chain and Lowe's scheme: Γ = 4.5, 22 and 45.0

The Schmidt number results presented in Fig. 6 motivate the re-calculation of the mean fractional extension of a wormlike chain molecule under shear. More specifically, since the parameter Γ controls the Schmidt number, and all the calculations in section 6 were done with $\Gamma = 4.5$ ($Sc \approx 35$), we repeat one case (the 5-bead chain) for $\Gamma = 22$ and 45. These values correspond to the more realistic $Sc \approx 690$ and 2574, respectively, at $k_BT = 0.2$. Figure 10 shows a much better agreement of the averaged values with the experimental data, verifying the consistency of the viscosity and diffusion calculations and the powerful alternative Lowe's scheme provides through the adjustment of Γ. Moreover, of interest is the monotonic dependence of the curves on Sc.

9. Summary

We have presented an outline of Lowe's DPD integrating scheme, a powerful alternative to existing schemes, such as the widely used velocity-Verlet method. Direct comparison with experimental data of λ-DNA molecules in uniform shear flow was performed and reasonable agreement between DPD, BD simulations and experiments was achieved. The advantages of the method become apparent when one computes the diffusion and viscosity of Lowe's fluid, which give realistic Schmidt number values, adjustable through one parameter Γ in the scheme. By determining an appropriate Schmidt number and the corresponding value for Γ, we revisited the problem of chains subject to wormlike forcing under shear and we recovered a much closer agreement with the experimental data.

The results presented in this work were generated using a serial, custom-developed code, written in the C/C++ programming language. Most simulations were performed on a single-CPU Intel 3.40GHz workstation with 2GB available physical memory, and the wall-clock execution time ranging from 30 minutes to 5 days. The pairwise force calculations were done using a linked cell list [29] to reduce the computational cost of neighbor searching. The overall computational method is parallelizable under the same conditions standard Molecular Dynamics codes are.

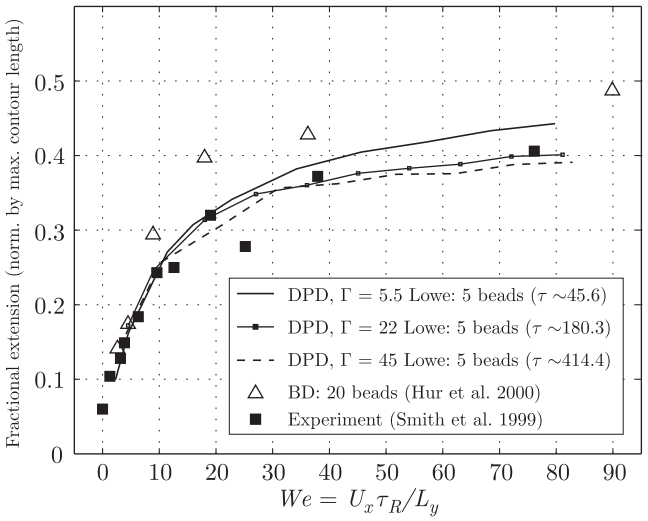

Fig. 10. Time-averaged mean fractional extension of a 5-beaded wormlike chain under shear versus We for $\Gamma = 4.5$ ($Sc \approx 35$), $\Gamma = 22$ ($Sc \approx 690$) and $\Gamma = 45$ ($Sc \approx 2574$). Here $k_BT = 0.2$. An empirical approximate formula would be $Sc \approx 1.4 \times \Gamma^2$, in agreement with Lowe's arguments [9]

References

[1] G.E. Karniadakis, A. Beskok, and N. Aluru, *Microflows and Nanoflows: Fundamentals and Simulation*, Springer, New York, 2005.

[2] X.B. Nie, S.Y. Chen, W.N.E and M.O. Robbins, A continuum and molecular hybrid method for micro- and nano-fluid flow, *J. Fluid Mech.* 500, 55–64 (2004).

[3] S. Succi, *The Lattice Boltzmann Equation for Fluid Dynamics and Beyond*, Oxford University Press, 2001.

[4] P.J. Hoogerbrugge and J.M. Koelman, "Simulating microscopic hydrodynamic phenomena with dissipative particle dynamics", *Europhys. Lett.* 19(3), 155–160 (1992).

[5] P. Español and P. Warren, "Statistical mechanics of dissipative particle dynamics", *Europhys. Lett.* 30(4), 191–196 (1995).

[6] B.M. Forrest and U.W. Suter, "Accelerated equilibration of polymer melts by time-coarse-graining", *J. Chem. Phys.* 102(18), 7256–7266 (1995).

[7] R.D. Groot and P.B. Warren, "Dissipative particle dynamics: Bridging the gap between atomistic and mesoscopic simulation", *J. Chem. Phys.* 107(11), 4423–4435 (1997).

[8] R.D. Groot and K.L. Rabone, "Mesoscopic simulation of cell membrane damage, morphology change and rupture by nonionic surfactants", *Biophys. J.* 81, 725–736 (2001).

[9] C.P. Lowe, "An alternative approach to dissipative particle dynamics", *Europhys. Lett.* 47(2), 145–151 (1999).

[10] L. Verlet, "Computer 'experiments' on classical fluids. I: Thermodynamical properties of Lennard-Jones molecules", *Phys. Rev.* 159, 98–103 (1967).

[11] P. Nikunen, M. Karttunen, and I. Vattulainen, "How would you integrate the equations of motion in dissipative particle dynamic simulations?", *Computer Physics Communications* 153, 407–423 (2003).

[12] H.C. Andersen, "Molecular dynamics simulations at constant pressure and/or temperature", *J. Chem. Phys.* 72(4), 2384–2396 (1980).

[13] E.A.J.F. Peters, "Elimination of time step effects in DPD", *Europhys. Lett.* 66(3), 311–317 (2004).

[14] O. Kratky and G. Porod, "Röntgenuntersuchung gelöster fadenmoleküle, *Rec. Trav. Chim.* 68, 1106–1115 (1949).

[15] H. Yamakawa, *Modern Theory of Polymer Solutions*, Harper and Row, New York, 1971.

[16] S.F. Sun, *Physical Chemistry of Macromolecules*, John Wiley & Sons, 1994.

[17] J.F. Marko and E.D. Siggia, "Stretching DNA", *Macromolecules* 28, 8759–8770 (1995).

[18] R.G. Larson, T.T. Perkins, D.E. Smith, and S. Chu, "Hydrodynamics of a DNA molecule in a flow field", *Phys. Rev. E* 55(2), 1794–1797 (1997).

[19] P.T. Underhill and P.S. Doyle, "On the coarse-graining of polymers into bead-spring chains", *J. Non-Newtonian Fluid Mech.* 122(1), 3–31 (2004).

[20] C. Bouchiat, M.D. Wang, J.F. Allemand, T. Strick, S.M. Block, and V. Croquette, "Estimating the persistence length of a worm-like-chain molecule from force-extension measurements", *Biophys. J.* 76, 409–413, (1999).

[21] D.E. Smith, H.P. Babcock, and S. Chu, "Single polymer dynamics in steady shear flo", *Science* 283, 1724 (1999).

[22] J.S. Hur, E.S.G. Shaqfeh, and R.G. Larson, "Brownian dynamics simulations of single DNA molecules in shear flow", *J. Rheol.* 44(4), 713–742 (2000).

[23] R.M. Jendrejack, J.J. de Pablo, and M.D. Graham, "Stochastic simulations of DNA in flow: dynamics and the effects of hydrodynamic interactions", *J. Chem. Phys.* 116, 7752–7759 (2002).

[24] A.W. Lees and S.F. Edwards, "The computer study of transport processes under extreme conditions, *J. Phys. C* 5, 1921 (1972).

[25] J.H. Irving and J.G. Kirkwood, "The statistical mechanical theory of transport processes. IV. The equations of hydrodynamics", *J. Chem. Phys.* 18, 817–829 (1950).

[26] J.A. Backer, C.P. Lowe, H.C.J. Hoefsloot, and P.D. Iedema, "Poiseuille flow to measure the viscosity of particle model fluids", *J. Chem. Phys.* 122, 154503 (2005).

[27] V. Symeonidis, *Numerical Methods for Multi-scale Modeling of Non-Newtonian Flows*, Phd thesis, Brown University, 2006.

[28] C.A. Marsh, *Theoretical Aspects of Dissipative Particle Dynamics*, Phd thesis, University of Oxford, 1998.

[29] M.P. Allen and D.J. Tildesley, *Computer Simulation of Liquids*, Oxford University Press, 1989.